J. Fluid Mech. (2019), *vol.* 862, *pp.* 871–888. © Cambridge University Press 2019
doi:10.1017/jfm.2018.966

Thrust, drag and wake structure in flapping compliant membrane wings

Gali Alon Tzezana[1,†] **and Kenneth S. Breuer**[1]

[1]Brown University, School of Engineering, Providence, RI 02912, USA

(Received 10 August 2018; revised 25 October 2018; accepted 23 November 2018; first published online 15 January 2019)

We present a theoretical framework to characterize the steady and unsteady aeroelastic behaviour of compliant membrane wings under different conditions. We develop an analytic model based on thin airfoil theory coupled with a membrane equation. Adopting a numerical solution to the model equations, we study the effects of wing compliance, inertia and flapping kinematics on aerodynamic performance. The effects of added mass and fluid damping on a flapping membrane are quantified using a simple damped oscillator model. As the flapping frequency is increased, membranes go through a transition from thrust to drag around the resonant frequency, and this transition is earlier for more compliant membranes. The wake also undergoes a transition from a reverse von Kármán wake to a traditional von Kármán wake. The wake transition frequency is predicted to be higher than the thrust–drag transition frequency for highly compliant wings.

Key words: flow–structure interactions, propulsion, swimming/flying

1. Introduction

Numerous animals including fish, whales, dolphins, birds, bats and insects use appendages (fins and wings) with varying levels of flexibility and/or compliance, to provide propulsion and/or weight support as they move through either air or water (e.g. Childress 1981; Blake 1983). Scientists have explored many different aspects of biological swimming and flying, such as flapping and flexibility effects, in an attempt to understand the underlying physical mechanisms and to apply them to engineering applications. Compliant membranes, used by bats, flying squirrels, lemurs and other animals define a specific subset of this class of flexible aerodynamic structures. These wings are of particular interest due to their negligible thicknesses and large shape deformations in both steady and unsteady conditions. In this paper, we discuss the aerodynamic characteristics of a flapping, compliant membrane wing.

1.1. *Fixed membrane wings*

The analysis of membrane wings dates back to the classical work of Thwaites (1961) and Nielsen (1963), who derived and solved the ‘sail equation’, which describes the relationship between tension, aerodynamic load and deflection for inextensible sails. Newman (1987) provides a review of these early works, which use attached

† Email address for correspondence: gali_alon@brown.edu

https://doi.org/10.1017/jfm.2018.966 Published online by Cambridge University Press

potential flow to predict the steady membrane shape. More recently, Smith & Shyy (1995*b*, 1996) developed a computational model for the coupled membrane and fluid (Navier–Stokes) equations, and used it to obtain steady solutions for extensible membranes with and without pretension, as well as for inextensible membranes with excess length. Comparing their full viscous solution with a potential-based model and with experimental results, they showed that a potential flow model can provide a good solution for small camber and incidence angles.

Song *et al.* (2008) suggested a simple analytic model linking the steady membrane deformation to the aerodynamic force. By assuming that load distribution is uniform, a simple expression for the maximum camber versus coefficient of lift was found to agree surprisingly well with experimental data over a wide range of aerodynamic and membrane prestretch conditions. They also demonstrated that, due to their self-cambering property, compliant membrane wings exhibit several beneficial characteristics, such as a steeper lift slope, larger maximum lift coefficient and delayed and softer stall characteristics as compared with their inextensible counterparts. Waldman & Breuer (2017) further expanded Song *et al.*'s approach by adding an inviscid, aerodynamic model for the coefficient of lift (assuming a Joukowski airfoil) while maintaining the uniform load assumption. This allowed maximum camber to be predicted with surprising good fidelity, knowing only the membrane and fluid properties and the angle of attack.

1.2. *Rigid flapping wings*

Forces associated with flapping (either heaving and/or pitching) rigid foils have been extensively studied experimentally (e.g. Triantafyllou, Triantafyllou & Gopalkrishnan 1991; Godoy-Diana, Aider & Wesfreid 2008; Bohl & Koochesfahani 2009), theoretically (e.g. Theodorsen 1935; Garrick 1936; Fernandez-Feria 2016) and numerically (e.g. Das, Shukla & Govardhan 2016; Deng *et al.* 2016; Andersen *et al.* 2017), yielding an extensive body of literature outlining flow regimes associated with both propulsion and drag. In potential flow, and allowing for vortex shedding, a rigid, heaving foil generates thrust at all frequencies, while a pitching foil generates drag at low frequencies, which transitions to thrust as the frequency is increased (Garrick 1936). At low Reynolds numbers, rigid foils operated in pure heave or pure pitch experience drag at low frequencies due to viscous effects (Das *et al.* 2016). In a combination of pitching and heaving motion, the propulsion/drag depends on the phase difference between pitching and heaving (Jones & Platzer 1997).

1.3. *Flexible flapping wings*

The introduction of flexibility adds a new degree of complexity, and most efforts have focused on inextensible structures with a finite bending stiffness actuated at the leading edge, but free to move at the trailing edge. We refer to these as flexible plates, in contrast to compliant membranes, that are extensible but with zero bending stiffness. Numerous studies have identified enhanced propulsive performance associated with a finite bending stiffness (e.g. Heathcote & Gursul 2007; Dewey *et al.* 2013; Moored *et al.* 2014; Quinn, Lauder & Smits 2015; Olivier & Dumas 2016; Paraz, Schouveiler & Eloy 2016). Similarly, for the less-studied case of flapping, compliant membrane wings with both leading and trailing edge support and zero bending stiffness, compliance has been shown to increase the average lift (Attar *et al.* 2011), thrust and efficiency (Banerjee & Patil 2008; Jaworski & Gordnier 2012, 2015), as compared to rigid wings. All of these studies on flapping membranes

https://doi.org/10.1017/jfm.2018.966 Published online by Cambridge University Press

focused on relatively low flapping frequencies, well below any resonant frequency inherent in the structure. Flapping flexible plates were shown to exhibit a peak in thrust at the resonant frequency (e.g. Michelin & Llewellyn Smith 2009; Moore 2014, 2015; Paraz *et al.* 2016; Moore 2017). However, increasing the flexibility, so that the flapping frequency lies above the resonance frequency, results in a transition to drag, as observed in the numerical simulation by Michelin & Llewellyn Smith (2009) and in the analytical model by Moore (2014).

There have also been some efforts to develop theoretical models for the fluid–structure interaction with flapping flexible foils, which may shed light on the underlying physics without the need for a time-consuming, high fidelity numerical simulation. Alben (2008, 2009) proposed such a model based on potential flow theory with a vortex sheet wake coupled with a structural beam model. More recently, Moore (2014, 2015, 2017) suggested a more computationally efficient formulation for the problem, where the coupling is based on pressure instead of vorticity. In recent work by Medina & Kang (2018), an analytic solution allows closed-form expressions for the lift, thrust and required input power to the problem of a flapping elastic plate. These low-amplitude models allow for extensive exploration of basic mechanisms in the fluid–structure interaction, including the improved aerodynamic performance around resonance, and the degradation in performance at higher flapping frequencies. However, to our knowledge, no such model has been extended to compliant tension-dominated membranes.

1.4. *Damped resonant systems*

It is also useful to analyse the problem of a flapping flexible or compliant wing in terms of a damped resonant system. Even in the absence of structural damping, the interaction with the fluid introduces added damping (as well as added mass) which may have a significant effect on the system response. A common approach to incorporate these forces is by using the semi-empirical Morison equation (Morison, Johnson & Schaaf 1950; Kang & Shyy 2014). In this formulation, the added mass effect is based on an analytic solution for a heaving, rigid plate (Katz & Plotkin 2001), while the damping term is assumed to be quadratic in velocity, accounting for the effect of inertial fluid forces due to the transverse motion of the wing. In these models, the damping coefficient is found empirically, and may be a function of the Reynolds number, flapping frequency and flapping amplitude. Richards & Oshkai (2015) performed a damped oscillator analysis on a flapping flexible foil, and replaced the quadratic damping term with an equivalent linear term, which is simpler mathematically but maintains the energy dissipation over a flapping cycle. They were able to fit this model to experimental results, and used it to explain trends in the propulsive performance; for example, the higher thrust of stiffer and heavier foils, when compared to more flexible and lighter foils with equivalent resonant frequency. Alben (2008) also analysed the motion of a pitching flexible foil as a damped resonant system, using an analytical model. In the limit of large reduced frequency, he found that the damping coefficient scales with $1/k$, where k is the reduced frequency.

1.5. *Wake structure*

The generation of thrust or drag by any flapping structure is also reflected in a vortex wake structure; traditionally, drag is associated with a von Kármán vortex wake while thrust is associated with a reverse von Kármán wake (Pederzani & Haj-Hariri 2006).

https://doi.org/10.1017/jfm.2018.966 Published online by Cambridge University Press

However, it has been observed that in some cases the transition between thrust and drag does not coincide with the transition in the wake structure. Godoy-Diana *et al.* (2008) used particle image velocimetry (PIV) to explore the wake structure and the propulsive performance of a pitching rigid foil, and reported that the transition in the wake structure precedes the thrust/drag transition. This has been confirmed by Bohl & Koochesfahani (2009), who measured the thrust from the measured velocity field using a control-volume approach which accounted for the unsteady fluctuations in velocity and pressure. Recent numerical studies on pure pitching and pure heaving rigid foils (Das *et al.* 2016; Deng *et al.* 2016) at low Reynolds numbers ($Re \leqslant 2000$) also showed that the thrust/drag transition frequency exceeds the one for wake structure transition.

The focus of the current paper is to extend the approach of Moore (2014, 2015, 2017) to the case of compliant membrane wings over a wide range of parameters that define the structural and flapping conditions. Using this approach we will explore the thrust/drag characteristics of these wings, and its relationship to the vortex wake structure. In § 2, we outline a general theoretical approach for treating the fluid–structure interaction with compliant membranes, both at a fixed angle of attack and subject to sinusoidal heaving and/or pitching motions. We use a high-order numerical technique to solve the resulting system of linear ordinary differential equations. In the current manuscript we only consider the cases of static, and heaving wings. The effect of wing compliance, inertia and flapping frequency are systematically explored in § 3, where we also develop a simple damped oscillator model to quantify the effects of added mass and fluid damping on the flapping membrane. The semi-empirical analytic model is used to characterize the behaviour near resonance, identifying the resonant frequency, added mass and fluid damping, as well as the conditions governing the generation of thrust or drag.

2. Analytic formulation

Consider a one-dimensional, linear elastic membrane wing of chord c in a uniform flow field with free-stream velocity U_∞. The leading and trailing edges of the membrane may be stationary, or perform a prescribed periodic motion as illustrated in figure 1. In general, the membrane deflection, $\hat{w}(\hat{x}, \hat{t})$, is governed by the nonlinear, unsteady structural equation (Smith & Shyy 1995*a*; Gordnier 2009):

$$\rho_m h \frac{\partial^2 \hat{w}}{\partial \hat{t}^2} - \tau\kappa = \Delta\hat{p}(\hat{x}, \hat{t}), \tag{2.1}$$

where ρ_m, h, τ and κ are the membrane density, thickness, tension and curvature, respectively, and we denote dimensional variables using the hat symbol. $\Delta\hat{p}$ is the aerodynamic pressure acting on the membrane, which is obtained using thin airfoil theory, and will be described below. The curvature, κ, and the tension, τ, of the membrane can be expressed in terms of its deflection, $\hat{w}(x)$:

$$\kappa = \frac{\partial^2 \hat{w}}{\partial \hat{x}^2} \left[1 + \left(\frac{\partial \hat{w}}{\partial \hat{x}}\right)^2\right]^{-3/2}, \tag{2.2}$$

$$\tau = Eh \left[\frac{\lambda_0}{c} \int_{-c/2}^{c/2} \sqrt{1 + \left(\frac{\partial \hat{w}}{\partial \hat{x}}\right)^2}\, \mathrm{d}\hat{x} - 1\right], \tag{2.3}$$

https://doi.org/10.1017/jfm.2018.966 Published online by Cambridge University Press

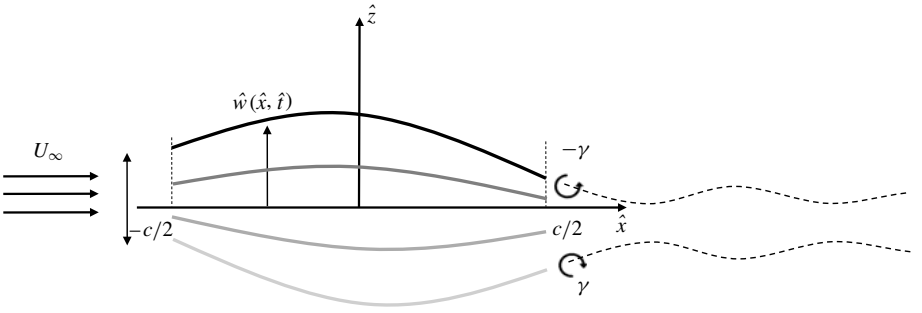


FIGURE 1. Schematic of the flapping membrane wing. The shading of the membrane indicate the different phases of the flapping cycle. A reverse von Kármán street is shed behind the membrane, illustrated by a dashed line. Although the theoretical model assumes that the wake lies along the x-axis, a wavy line is shown to represent the spatio-temporal fluctuations of vorticity.

where λ_0 is the membrane prestretch:

$$\lambda_0 = \frac{c}{L_0}, \tag{2.4}$$

and L_0 is the initial length of the membrane.

We scale all parameters with the half-chord, $c/2$, and the convective time scale, $c/(2U_\infty)$; pressure is scaled by the dynamic pressure, $\rho U_\infty^2/2$. The resulting non-dimensional equation for the membrane becomes:

$$4R\frac{\partial^2 w}{\partial t^2} - 2Ae\left[\frac{\lambda_0}{2}\int_{-1}^{1}\sqrt{1+\left(\frac{\partial w}{\partial x}\right)^2}\,\mathrm{d}x - 1\right]\left[1+\left(\frac{\partial w}{\partial x}\right)^2\right]^{-3/2}\frac{\partial^2 w}{\partial x^2} = \Delta C_p, \tag{2.5}$$

where the aeroelastic number, Ae, and the mass ratio, R, are given by:

$$Ae = \frac{Eh}{\frac{1}{2}\rho U_\infty^2 c}, \quad R = \frac{\rho_m h}{\rho c}. \tag{2.6a,b}$$

To solve this equation, we explore two limiting cases. Firstly, we take the time derivative to be zero and solve the case of a steady membrane at a fixed angle of attack. Secondly, we linearize the unsteady problem to study a membrane flapping at low amplitude. Details of the two solutions are given below.

2.1. *Steady membrane at fixed angle of attack*

In the steady case, the membrane equation (2.1) reduces to the Young–Laplace equation, which governs the static equilibrium shape of a membrane under a pressure load (see Waldman & Breuer 2017):

$$\kappa + \frac{\Delta\hat{p}}{\tau} = 0. \tag{2.7}$$

https://doi.org/10.1017/jfm.2018.966 Published online by Cambridge University Press

In non-dimensional form, the Young–Laplace equation (2.7) is written:

$$\frac{\mathrm{d}^2 w}{\mathrm{d}x^2} = -\Delta C_p \left[1 + \left(\frac{\mathrm{d}w}{\mathrm{d}x}\right)^2\right]^{3/2} \cdot \left\{2Ae\left[\frac{\lambda_0}{2}\int_{-1}^{1}\sqrt{1+\left(\frac{\mathrm{d}w}{\mathrm{d}x}\right)^2}\,\mathrm{d}x - 1\right]\right\}^{-1}. \quad (2.8)$$

In the present analysis, the pressure term, ΔC_p, is obtained from thin airfoil theory (Katz & Plotkin 2001) for a given angle of attack α. Using the transformation $x = -\cos\theta$, the pressure coefficient can be written as:

$$\Delta C_p = 4\left[\left(\alpha - \frac{1}{\pi}\int_0^{\pi}\frac{\mathrm{d}w}{\mathrm{d}x}\,\mathrm{d}\theta\right)\cot\frac{\theta}{2} + \frac{2}{\pi}\sum_{n=1}^{\infty}\left(\int_0^{\pi}\frac{\mathrm{d}w}{\mathrm{d}x}\cos n\theta\,\mathrm{d}\theta\cdot\sin n\theta\right)\right]. \quad (2.9)$$

The structural and aerodynamic equations ((2.8) and (2.9)), together with the boundary conditions $w(0) = w(1) = 0$, are solved iteratively using a Chebyshev collocation method (Mason & Handscomb 2002) for any combination of the input parameters: the angle of attack, α, the membrane prestretch, λ_0, and the aeroelastic number, Ae.

2.2. *Pitching and heaving membrane*

For the unsteady case, we linearize the membrane equation (2.5) for small deflections:

$$4R\frac{\partial^2 w}{\partial t^2} - 2Ae(\lambda_0 - 1)\frac{\partial^2 w}{\partial x^2} = \Delta C_p. \quad (2.10)$$

The leading and trailing edges of the membrane perform a periodic motion of reduced frequency $k = \pi\hat{f}c/U_\infty$, where $\hat{f}$ is the dimensional frequency.

Following Wu (1961), the pressure difference across the membrane is obtained from unsteady thin airfoil theory, under the assumptions of two-dimensional potential flow with small-amplitude deflections. The model includes the shedding of a planar vortex wake from the trailing edge. We assume the wing is performing time-harmonic motion of the form:

$$w(x,t) = W(x)\mathrm{e}^{jkt} = \left[\frac{\beta_0}{2} + \sum_{n=1}^{\infty}\beta_n\cos(n\theta)\right]\mathrm{e}^{jkt}, \quad (2.11)$$

in which case the resulting pressure jump on the membrane is also time harmonic and given by $\Delta C_p(x,t) = P(x)\mathrm{e}^{jkt}$, where

$$P(x) = a_0\sqrt{\frac{1-x}{1+x}} + 2\sum_{n=1}^{\infty}a_n\sin(n\arccos x) \quad (2.12)$$

and the coefficients, a_n, depend linearly on the deflection, $W(x)$ (Wu 1961; Moore 2014). Using this result from thin airfoil theory, (2.12), a linear ordinary differential equation (ODE) is obtained:

$$[-4Rk^2 - 2Ae(\lambda_0 - 1)\mathcal{D}^2]W(x) = P(x), \quad (2.13)$$

where $\mathcal{D} \equiv \mathrm{d}/\mathrm{d}x$.

https://doi.org/10.1017/jfm.2018.966 Published online by Cambridge University Press

Boundary conditions for a pitching and heaving wing are defined by the motion of the chord line, connecting the leading and trailing edges. After non-dimensionalization, linearization and the assumption of harmonic motion, these are given by:

$$\left.\begin{aligned} W(-1) &= A_0 + (1+x_h)\tan(\theta_0\cos(\phi)) - j(1+x_h)\tan(\theta_0\sin(\phi)),\\ W(1) &= A_0 - (1-x_h)\tan(\theta_0\cos(\phi)) + j(1-x_h)\tan(\theta_0\sin(\phi)),\end{aligned}\right\} \tag{2.14}$$

where the amplitude of the motion is defined by the heaving amplitude A_0, the pitching amplitude θ_0, the phase difference ϕ and the pitching reference point x_h. Note that these boundary conditions do not constrain the membrane angle at the leading and trailing edge. The current study focuses on membranes performing pure heaving motion ($\theta_0 = 0$). Since the unsteady analysis is linear, the normalized flapping amplitude, A_0, is arbitrary and chosen to be one for convenience. We note that the commonly used Strouhal number, $St = 2\hat{f}A_0/U_\infty$ (Triantafyllou *et al.* 1991), is equivalent to the reduced frequency, k.

The spatial ODE (2.13), together with the boundary conditions (2.14), is discretized using a Chebyshev collocation method, and the resulting linear system is solved iteratively, following the procedure described by Moore (2015, 2017). The solution is obtained using the generalized minimal residual method (GMRES) (Saad & Schultz 1986) with a tolerance of 10^{-12} and using 32 collocation points, which was confirmed to be sufficient to achieve fully resolved solutions.

Once the membrane deflections and the corresponding pressure distribution are obtained, we can find the lift and thrust acting on the membrane. The lift coefficient is calculated as $C_L = \int_{-1}^{1} \Delta C_p \,\mathrm{d}x$. The thrust coefficient is the sum of two components: $C_T = C_{T_P} + C_{T_S}$, where $C_{T_P} = \int_{-1}^{1} \Delta C_p(\partial w/\partial x)\,\mathrm{d}x$ results from pressure differences over the membrane, and C_{T_S} represents the leading edge suction (Wu 1961; Moore 2014). To evaluate the aerodynamic performance of the membrane, we calculate the maximum lift and average thrust coefficients over a cycle (note that the average lift over a heaving cycle is zero).

The aerodynamic model includes the shedding of a vortex sheet from the trailing edge, and its strength can be found from the tangential velocity jump across the wake (Wu 1961). The planar wake in this model has a sinusoidal vorticity distribution, and is advected downstream at the free-stream velocity. This leads to the following form of the vortex sheet strength:

$$\gamma_{wake} = H(k)\mathrm{e}^{jk[t-(x-1)]}, \tag{2.15}$$

where $H(k)$ is a complex transfer function relating the wake vorticity to the flapping motion. The phase of the transfer function determines the wake structure: if $\mathrm{Re}\{H(k)\} < 0$ (or a phase between $\pi/2$ and $3\pi/2$), then the shed vorticity is negative at the beginning of the downstroke and positive at the beginning of the upstroke, corresponding to a reverse von Kármán wake that is generally associated with thrust. This case is illustrated in figure 1. Conversely, $\mathrm{Re}\{H(k)\} > 0$ corresponds to a 'regular' von Kármán wake, generally associated with drag. A transition in the wake structure is identified as $\angle H(k) = \pi/2$.

3. Results and discussion

3.1. *Steady membrane at fixed angle of attack*

As suggested by Song *et al.* (2008), a useful non-dimensional number to parameterize the deformation of a membrane is a Weber number, which compares the aerodynamic

https://doi.org/10.1017/jfm.2018.966 Published online by Cambridge University Press

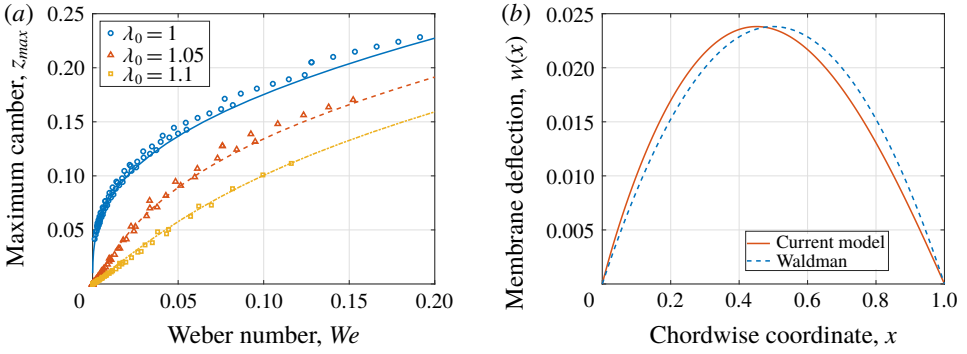


FIGURE 2. (Colour online) (*a*) Variation of maximum camber with Weber number, for different prestretch values. Symbols: current model, solid lines: model by Waldman & Breuer (2017). There is good agreement between the two models, validating the assumption of a uniform-pressure distribution along the chord. (*b*) Difference in membrane shape between the model by Waldman & Breuer (2017), assuming uniform-pressure distribution, and the current model. Solution obtained for $\alpha = 3°$, $Ae = 30$, $\lambda_0 = 1.1$.

pressure with the membrane tension:

$$We = \frac{F_L}{Eh} = \frac{C_L}{Ae}, \tag{3.1}$$

where F_L is the lift force per unit length, and C_L is the lift coefficient. Variation of the maximum camber with Weber number is presented in figure 2(*a*) for different values of prestretch, λ_0, and compared with the uniform-pressure model developed by Waldman & Breuer (2017). In that model, defining the aeroelastic number and the angle of attack uniquely determines both the maximum camber and the lift coefficient, and hence establishes a unique relationship between Weber number and maximum camber. However, in the current solution the lift coefficient also depends on the aeroelastic number through the coupled fluid–structure interaction. Therefore, different combinations of the aeroelastic number and the lift coefficient may lead to slightly different predictions of the maximum camber for the same value of the Weber number. This weak dependency was also seen by Waldman & Breuer (2017) in their numerical simulations that used XFOIL (Drela 1989) for the aerodynamic model coupled to a membrane model for the structure.

Nonetheless, there is good general agreement between the two models, validating the simplified assumption of a uniform pressure distribution, at least for predictions of maximum camber. Not surprisingly, the differences lie in the membrane's shape: while Waldman and Breuer's model assumes that the membrane has the form of a circular arc, the current model allows an arbitrary shape for the deflection, resulting in a more complex shape with the maximum camber closer to the leading edge (figure 2*b*).

3.2. *Heaving membrane*

The power of the current approach lies in its ability to predict the unsteady aero-mechanical performance of a compliant membrane. In order to explore the effect of the different parameters on the flapping membrane's performance, the aeroelastic number, Ae, the mass ratio, R, and the reduced frequency were varied

https://doi.org/10.1017/jfm.2018.966 Published online by Cambridge University Press

Study	$Re\,[\times 10^3]$	Ae	R	λ_0
Waldman & Breuer (2017)	30–80	10–220	1.3–2.6	1–1.1
Rojratsirikul *et al.* (2009)	50–100	190–770	1.1	1.025
Jaworski & Gordnier (2015)	2.5	614	1.2	1.05
Bat flight (Hubel *et al.* 2012; Cheney *et al.* 2014; Bergou *et al.* 2015; Skulborstad *et al.* 2015)	3–20	120	4	—
Current study	—	60–300	1–7	1.05

TABLE 1. Summary of parameter ranges used in previous and current studies.

over a wide range, summarized in table 1. This range includes the experiments conducted by Rojratsirikul, Wang & Gursul (2009) and Waldman & Breuer (2017), both of whom measured the deformations of a fixed membrane in air, the numerical simulation by Jaworski & Gordnier (2015) for a two-dimensional flapping membrane at a Reynolds number of 2500, as well as an estimate of the parameters representing a biological flyer – a bat during steady flight (Hubel *et al.* 2012; Cheney *et al.* 2014; Bergou *et al.* 2015; Skulborstad, Swartz & Goulbourne 2015).

3.2.1. *Membrane kinematics*

The deflections of a membrane in pure heave over half a cycle are presented in figure 3 for different values of the reduced frequency, k, normalized by the natural frequency, k_1, which is defined later (3.5). The amplitude of the membrane deflection is scaled by the amplitude of the leading and trailing edges' motions. The central column corresponds to a membrane flapping at a resonant frequency, where the deflections are visibly larger. Note that the phase of the membrane deflection with respect to the motion of the leading and trailing edges changes as the frequency passes through the resonant condition.

The maximum deflection throughout the flapping cycle is defined as the maximum difference, over a cycle, between the membrane position and the position of a rigid plate performing the same heaving motion: $Z_{max} = \max(w(x,\,t) - w_{rigid}(x,\,t))$. In figure 4, we display the maximum deflection for different values of the aeroelastic number (figure 4*a*) and mass ratio (figure 4*b*). For a low flapping frequency, the deflection in all cases is small, but increases with the reduced frequency until a resonant peak is observed. In some cases, a second and even third resonant peak is seen within the range of frequencies plotted.

The resonant frequency increases as the aeroelastic number is increased (figure 4*a*), and decreases when increasing the mass ratio (figure 4*b*). This suggests a connection between resonance and the natural frequency, as was also reported by Michelin & Llewellyn Smith (2009). It is also apparent that the width of the resonant peak, which is related to damping in the system, depends on the parameters. In particular, the damping appears to be larger for low values of the mass ratio, R.

To model the effect of the resonance and damping we employ a simple damped oscillator model, following the conceptual analysis suggested by Païdoussis, Price & de Langre (2010). Considering the membrane equation (2.10), we assume sinusoidal deflection modes. Focusing on the first resonant frequency, where the first mode $w(x,\,t) \approx \eta(t)\cos(\pi x/2)$ is dominant (figure 3), we can then write a forced damped oscillator equation for the amplitude of the first mode, $\eta(t)$:

$$4R\ddot{\eta} + \frac{\pi^2}{2}Ae(\lambda_0 - 1)\eta = F_f(\dot{\eta},\,\ddot{\eta}), \tag{3.2}$$

https://doi.org/10.1017/jfm.2018.966 Published online by Cambridge University Press

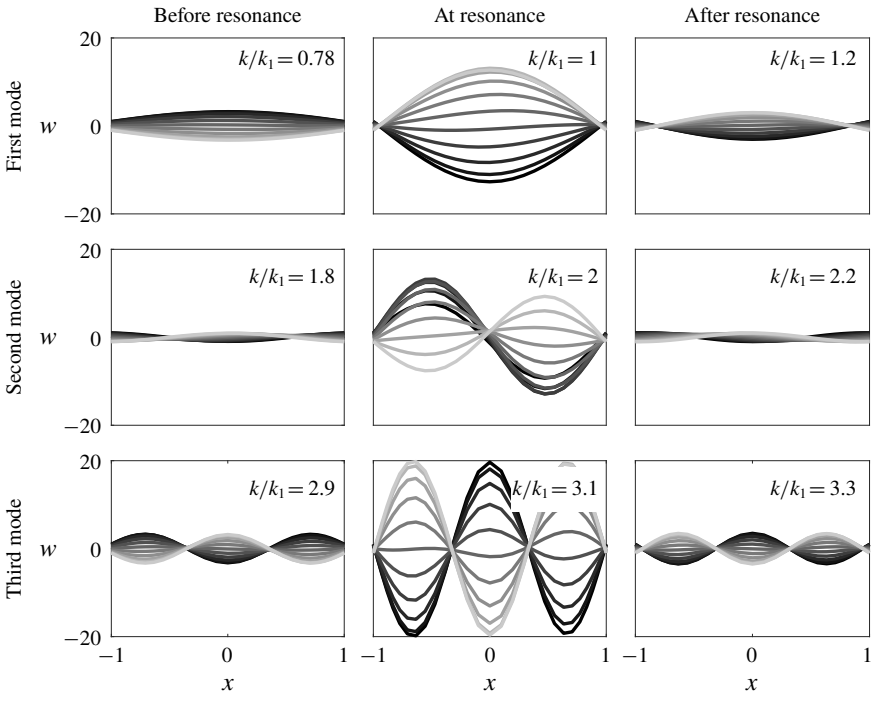


FIGURE 3. Membrane in pure heave, deflections during downstroke for different values of the normalized frequency k/k_1. Dark: beginning of the downstroke, $t/T = 0$; light: end of the downstroke, $t/T = 0.5$. Case parameters: $A_0 = 1$, $Ae = 120$, $\lambda_0 = 1.05$, $R = 4$, $k_1 = 1.3$. The different rows correspond to the first three resonant frequencies. For each row, the first plot is before resonant frequency, the middle plot is close to resonance (note the large deflections) and the third is after resonance. The different modes of vibrations become dominant at the different resonant frequencies. A phase shift in the membrane's deflection occurs as the membrane passes through resonance.

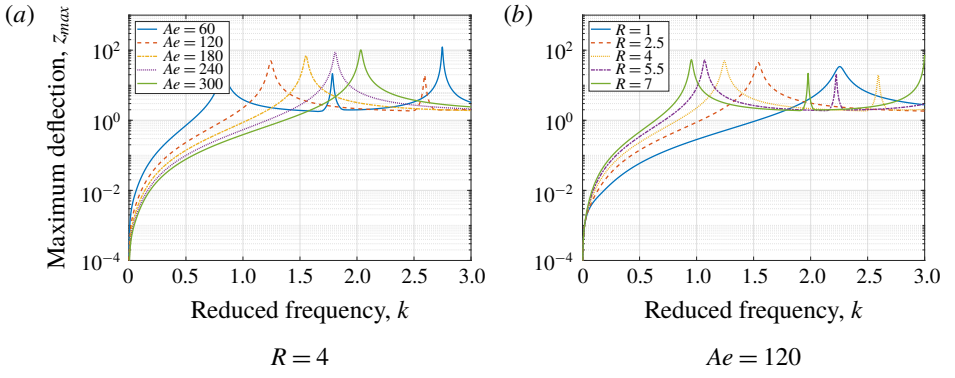


FIGURE 4. (Colour online) Membrane in pure heave, maximum deflection for different values of the reduced frequency k. A clear resonant peak is observed for all membranes, and for some the second and third resonances also appear in the plotted range of flapping frequencies. The resonant frequency increases as the aeroelastic number is increased, and decreases when increasing the mass ratio.

https://doi.org/10.1017/jfm.2018.966 Published online by Cambridge University Press

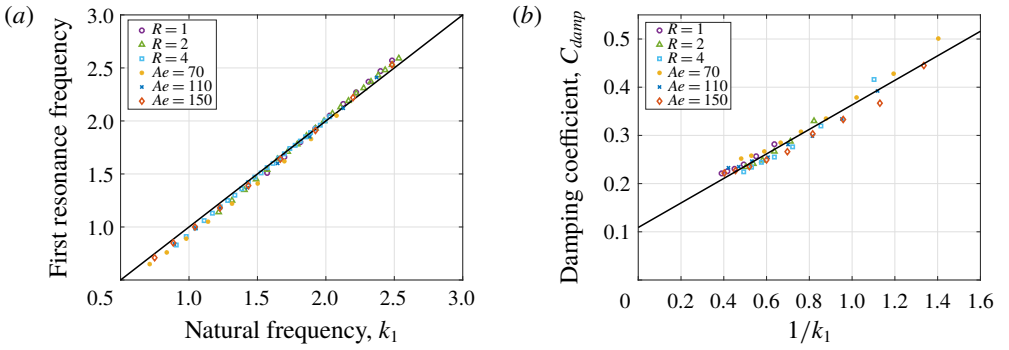


FIGURE 5. (Colour online) (*a*) Comparison of first resonant frequency with the membrane's natural frequency, for membranes with different values of the aeroelastic number and mass ratio. Symbols: current model, solid line: k_1. The added mass parameter is $R_A = 0.5$. (*b*) The damping coefficient, obtained from the deflection response using the half-power bandwidth method, plotted against $1/k_1$ for membranes with different parameters.

where F_f is the fluid forcing, which depends on the motion of the membrane. Suppose further that the fluid forcing, F_f, may be expressed as the sum of two terms, dependent on the acceleration and velocity of the membrane:

$$F_f(\dot{\eta}, \ddot{\eta}) = -4R_A\ddot{\eta} - 2C_{damp}\dot{\eta}, \tag{3.3}$$

where the first and the second term represent the added mass and the fluid damping, respectively. The coefficients R_A and C_{damp} are unknown, and may or may not be constant with respect to the relevant parameters of the system. Using this form for the fluid forcing, F_f, leads to the following damped oscillator equation:

$$2(R + R_A)\ddot{\eta} + C_{damp}\dot{\eta} + \frac{\pi^2}{4}Ae(\lambda_0 - 1)\eta = 0. \tag{3.4}$$

Here we can identify the respective mass, damping and stiffness coefficients of the total system, which consists of both the membrane and the surrounding fluid. The natural frequency of this oscillator is written as:

$$k_1 = \frac{\pi}{\sqrt{8}}\sqrt{\frac{Ae(\lambda_0 - 1)}{R + R_A}}. \tag{3.5}$$

By comparing the observed value for the first natural frequency, k_1, with the predicted value (3.5) we find that a value of $R_A = 0.5$ is able to collapse the data over a range of values for Ae and R (figure 5*a*). This is somewhat lower than the values calculated for a rigid heaving plate ($R_A = \pi/4$, Katz & Plotkin 2001) and for a vibrating membrane in still air ($R_A = 0.68$, Minami 1998). The current model cannot be used to estimate R_A for either a rigid plate or a membrane in still air, as these conditions lead to an infinite value of the aeroelastic number, and consequently, an infinite value of the natural frequency (3.5), regardless of the added mass coefficient.

https://doi.org/10.1017/jfm.2018.966 Published online by Cambridge University Press

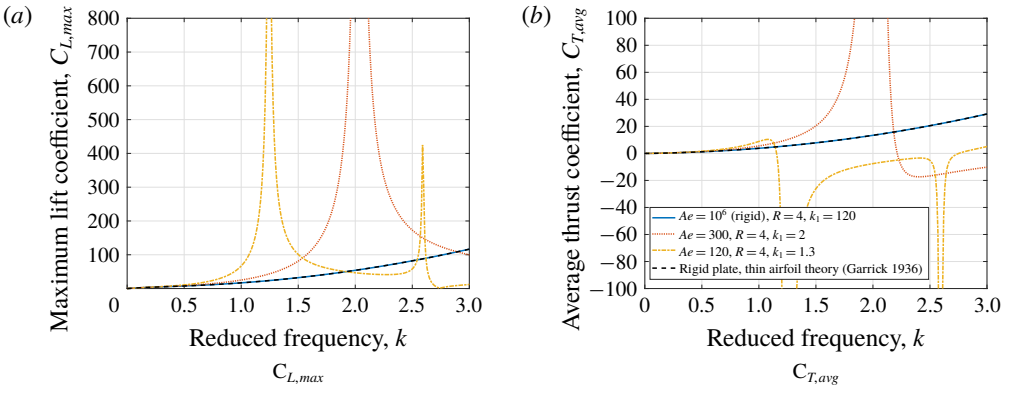


FIGURE 6. (Colour online) Variation of (*a*) maximum lift coefficient, and (*b*) average thrust coefficient with the reduced frequency for a membrane in pure heave; $A = 1$, $\lambda_0 = 1.05$, $R = 4$. The dashed line represents classical thin airfoil theory for a rigid plate (Garrick 1936), in agreement with the current model. Lift and thrust magnitude increase at the resonant frequency. A stiffer membrane (higher aeroelastic number, red) generates thrust at low frequencies, which increases at the resonant frequency and then drops and transitions to drag at a higher frequency. For a more compliant membrane (yellow), the transition from thrust to drag occurs earlier, below resonance.

From the simplified damped oscillator model (3.4) we can also find the relationship between the damping coefficient, C_{damp}, and the damping ratio, ζ:

$$2\zeta k_1 = \frac{C_{damp}}{2(R + R_A)}. \tag{3.6}$$

Using the half-power bandwidth method (Thomson 1996), we obtain the damping coefficient around the first resonance from the deflection response for the range of parameters tested. The damping coefficient was found to scale with $1/k_1$ (figure 5*b*). This is in agreement with Alben (2008) who developed an analytic model for a pitching flexible foil with a free trailing edge and found that, in the limit of large reduced frequency, the damping coefficient also scales with $1/k$.

3.2.2. *Aerodynamic performance*

In figure 6, the variation of the maximum lift and average thrust coefficients with the reduced frequency is shown for three cases: a rigid wing, a compliant wing with $Ae = 300$ and a very compliant wing with $Ae = 120$. The rigid wing solution agrees with the analytic solution by Garrick (1936). The two compliant wings show increase in the magnitude of the aerodynamic coefficients at resonance, although the average thrust response is quite different: the less compliant wing, $Ae = 300$, produces high thrust at resonance; in contrast, increasing the compliance, $Ae = 120$, results in drag production at resonance. A similar phenomenon was shown by Moore (2014) for a flexible wing with a free trailing edge and a torsional spring at the leading edge: as the spring's flexibility increases, the flapping wing produces less thrust at resonant frequency – even to the point of transition to drag.

To better understand the thrust–drag transition, we examine the wake structure behind the heaving membrane. In figure 7 we plot the phase of the transfer function, $H(k)$, (corresponding to wake structure, equation (2.15)) and the average thrust

https://doi.org/10.1017/jfm.2018.966 Published online by Cambridge University Press

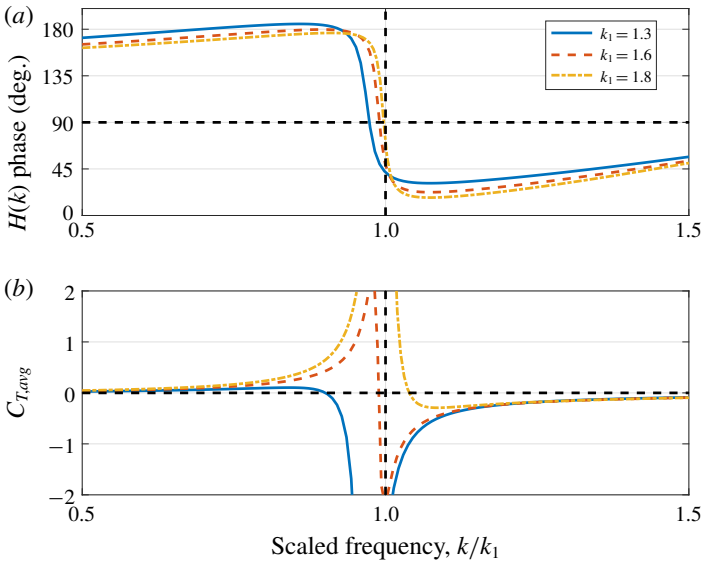


FIGURE 7. (Colour online) Variation of the phase of the wake transfer function (*a*) and the average thrust coefficient (*b*) with normalized frequency, k/k_1, for three different membranes. At a low flapping frequency, all membranes produce thrust and the corresponding reverse von Kármán wake is observed (identified by $\angle H(k) > 90°$). At a high frequency, the opposite happens – membranes have a regular von Kármán wake, and generate drag accordingly. Intersection with the dashed lines marks the transition in the wake structure (*a*) or transition from thrust to drag (*b*). For a very compliant membrane (low k_1), the thrust/drag transition occurs before the transition in the wake structure, and *vice versa*.

coefficient against the frequency, here normalized by the resonance frequency, k/k_1. The different membranes are identified using their natural frequency. At resonance, the wake transitions from a reverse von Kármán street, traditionally associated with thrust, to the regular von Kármán street associated with drag. This change of sign corresponds to a phase shift in the membrane's shape, as can be seen in figure 3 before and after the resonance (first and last columns). Accordingly, all membranes produce thrust at low frequencies ($k/k_1 \ll 1$, below resonance) and drag at high frequencies ($k/k_1 \gg 1$, above resonance). This is in agreement with the experimental results of Spagnolie *et al.* (2010) and the numerical simulation of Zhang, Liu & Lu (2010), who showed that a self-propelled, passively pitching plate moves forward when driven below the natural frequency, and backward when driven at a frequency higher than the natural frequency. However, the thrust–drag transition does not coincide with the transition in the wake, as was also observed in the experiments of Godoy-Diana *et al.* (2008), and in the numerical simulation by Michelin & Llewellyn Smith (2009). As the membrane's natural frequency, k_1, decreases, the transition to drag occurs at a lower frequency, resulting in a peak in drag at the resonance condition.

The thrust/drag and wake transition frequencies depend on the natural frequency, k_1, as shown in figure 7, but also on the parameters Ae and R. As shown in figure 8, membranes with the same natural frequency may have different thrust/drag and wake transition frequencies. This is due to the effect of fluid damping, which becomes more

https://doi.org/10.1017/jfm.2018.966 Published online by Cambridge University Press

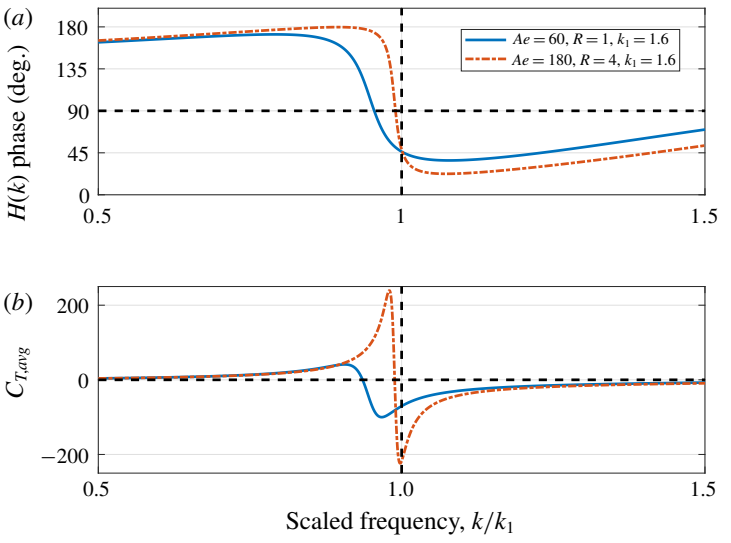


FIGURE 8. (Colour online) Variation of the phase of the wake transfer function (*a*) and the average thrust coefficient (*b*) with the normalized frequency, k/k_1, for two different membranes with the same natural frequency. Varying the aeroelastic number and the mass ratio changes the effect of fluid damping, which becomes dominant as the parameters become small. This results in a change in the thrust/drag and wake transition frequencies.

dominant for a high aeroelastic number and mass ratio. This was also observed by Richards & Oshkai (2015) for flapping flexible foils. We can use a scaling argument to understand this effect. As can be derived from (3.6), the damping ratio, ζ, is proportional to $1/(Rk_1^2)$, and so a heavier membrane (relative to the fluid), i.e. one with a higher value of R, would experience less damping even if the natural frequency is kept constant.

Figure 9 shows the variation with natural frequency of the wake transition frequency (*a*) and the thrust/drag transition frequency (*b*), both normalized by the natural frequency, k_1. Over the entire parameter range, the transition in the wake structure occurs close to the natural (resonant) frequency, with just a slight decrease at lower values of k_1. However the thrust/drag transition may occur before or after resonance, depending on the natural frequency. If inertia is dominant (low k_1, more compliant wing), transition from thrust to drag happens before resonance ($k_{thrust}/k_1 < 1$). However when stiffness dominates (high k_1) we continue to generate thrust at higher frequencies. At the limit of a heaving rigid plate ($k_1 \to \infty$) thin airfoil theory predicts thrust at all flapping frequencies (Garrick 1936).

4. Conclusions

We have presented an analytic model for the steady and unsteady fluid–structure interactions with compliant membrane wings. We solve the coupled aerodynamic and structural models using a Chebyshev collocation method. The model, which extends the approach used by Moore (2014, 2015, 2017) for elastic plates in a flow, allows us to investigate the effects of inertia, compliance and flapping kinematics on the steady and dynamic response of the membrane.

The steady model retains a level of simplicity so that large scale simulations can be avoided, but improves upon a previous model by Waldman & Breuer (2017),

https://doi.org/10.1017/jfm.2018.966 Published online by Cambridge University Press

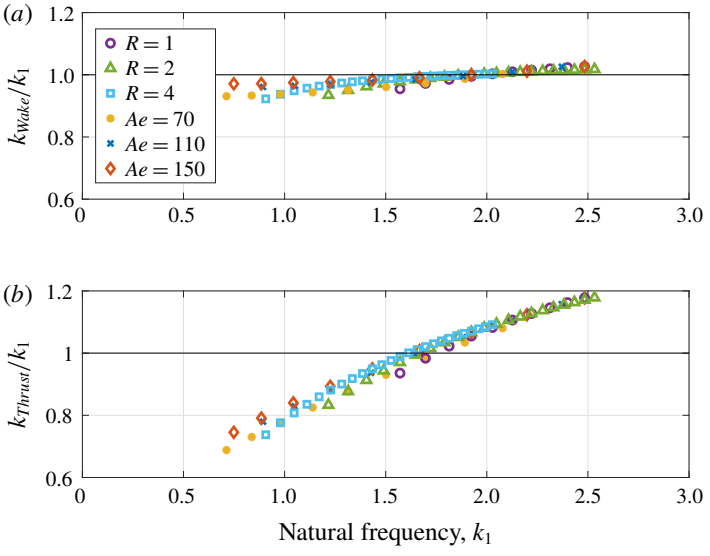


FIGURE 9. (Colour online) (*a*) Wake transition and (*b*) thrust/drag transition frequencies normalized by the natural frequency, plotted as a function of the natural frequency. Transition in the wake structure occurs close to the natural (resonant) frequency. If inertia is dominant (low k_1, more compliant wing), transition from thrust to drag happens before resonance; however when stiffness dominates (high k_1), we can get thrust for higher frequencies, to the limit of a rigid plate that produces thrust at any flapping frequency (Garrick 1936).

by incorporating thin airfoil theory for the aerodynamic model. Good agreement is observed in the maximum deflection of the membrane between the two models, despite small variations in the predicted membrane shape.

For the case of a flapping membrane wing, we explored the kinematics and propulsive properties of heaving membranes with varying compliance, inertia and flapping frequencies. A simple damped oscillator model allowed us to quantify the effects of added mass and fluid damping on a flapping membrane. The added mass coefficient was found to be constant over a range of parameters, and slightly lower than previous estimations for rigid plates and for membranes in still fluid. The fluid damping coefficient around the first resonance scales as $1/k_1$, where k_1 is the system's natural frequency.

Resonance occurs when flapping at the system's natural frequency, characterized by a peak in the maximum deflection and the aerodynamic coefficients. The thrust coefficient at resonance reaches a maximum for relatively rigid membranes, but highly compliant membranes may produce drag at resonance. While the transition of the wake from a reverse von Kármán street to the traditional von Kármán street occurs at the resonant frequency, the transition from thrust to drag depends on natural frequency, being earlier for membranes with a low natural frequency (very compliant or heavy membranes), and later when the natural frequency is high (for lighter or more rigid membranes).

The approach clearly has its limitations. The linear assumptions break down for large deflections, and this will certainly modify the predictions near the resonant conditions. In addition, the effects of viscosity, which in real life introduces boundary

https://doi.org/10.1017/jfm.2018.966 Published online by Cambridge University Press

layer transition to turbulence and separation, will also limit the applicability of the model. The 'spring–mass–damper' model introduces yet further simplifications. Nevertheless, similar analytic and low-order models have been shown to have wide interpretative and predictive utility in the unsteady aerodynamics, animal locomotion and flapping flag communities. Despite their limitations, these models provide valuable physical insight and we anticipate that the same will be true with this approach, although experimental validation (currently planned) is needed to determine the range over which these predictions are of value.

Acknowledgements

This research was supported by a collaborative research agreement with the Government of Israel and by a research grant from the US Army Natick Soldier Systems Center. Many thanks go to the individuals of the Breuer Lab for valuable discussion and technical assistance.

REFERENCES

ALBEN, S. 2008 Optimal flexibility of a flapping appendage in an inviscid fluid. *J. Fluid Mech.* **614**, 355–380.

ALBEN, S. 2009 Simulating the dynamics of flexible bodies and vortex sheets. *J. Comput. Phys.* **228** (7), 2587–2603.

ANDERSEN, A., BOHR, T., SCHNIPPER, T. & WALTHER, J. H. 2017 Wake structure and thrust generation of a flapping foil in two-dimensional flow. *J. Fluid Mech.* **812**, R4.

ATTAR, P. J., GORDNIER, R. E., JOHNSTON, J. W., ROMBERG, W. A. & PARTHASARATHY, R. N. 2011 Aeroelastic analysis of membrane microair vehicles. Part II. Computational study of a plunging membrane airfoil. *J. Vib. Acoust.* **133** (2), 021009.

BANERJEE, S. & PATIL, M. 2008 Aeroelastic analysis of membrane wings. In *49th AIAA/ASME/ASCE/AHS/ASC Structures, Structural Dynamics, and Materials Conference*, p. 1812. American Institute of Aeronautics and Astronautics.

BERGOU, A. J., SWARTZ, S. M., VEJDANI, H., RISKIN, D. K., REIMNITZ, L., TAUBIN, G. & BREUER, K. S. 2015 Falling with style: bats perform complex aerial rotations by adjusting wing inertia. *PLoS Biol.* **13** (11), 1–16.

BLAKE, R. 1983 *Fish Locomotion*. Cambridge University Press.

BOHL, D. G. & KOOCHESFAHANI, M. M. 2009 MTV measurements of the vortical field in the wake of an airfoil oscillating at high reduced frequency. *J. Fluid Mech.* **620**, 63–88.

CHENEY, J. A., KONOW, N., MIDDLETON, K. M., BREUER, K. S., ROBERTS, T. J., GIBLIN, E. L. & SWARTZ, S. M. 2014 Membrane muscle function in the compliant wings of bats. *Bioinspir. Biomim.* **9** (2), 025007.

CHILDRESS, S. 1981 *Mechanics of Swimming and Flying*. Cambridge University Press.

DAS, A., SHUKLA, R. K. & GOVARDHAN, R. N. 2016 Existence of a sharp transition in the peak propulsive efficiency of a low-pitching foil. *J. Fluid Mech.* **800**, 307–326.

DENG, J., SUN, L., TENG, L., PAN, D. & SHAO, X. 2016 The correlation between wake transition and propulsive efficiency of a flapping foil: a numerical study. *Phys. Fluids* **28** (9), 094101.

DEWEY, P. A., BOSCHITSCH, B. M., MOORED, K. W., STONE, H. A. & SMITS, A. J. 2013 Scaling laws for the thrust production of flexible pitching panels. *J. Fluid Mech.* **732**, 29–46.

DRELA, M. 1989 Xfoil: an analysis and design system for low Reynolds number airfoils. In *Low Reynolds Number Aerodynamics* (ed. T. J. Mueller), Lecture Notes in Engineering, vol. 54. Springer.

FERNANDEZ-FERIA, R. 2016 Linearized propulsion theory of flapping airfoils revisited. *Phys. Rev. Fluids* **1** (8), 084502.

GARRICK, I. E. 1936 Propulsion of a flapping and oscillating airfoil. *NACA Tech. Rep.* 567.

https://doi.org/10.1017/jfm.2018.966 Published online by Cambridge University Press

GODOY-DIANA, R., AIDER, J.-L. & WESFREID, J. E. 2008 Transitions in the wake of a flapping foil. *Phys. Rev.* E **77** (1), 016308.

GORDNIER, R. E. 2009 High fidelity computational simulation of a membrane wing airfoil. *J. Fluids Struct.* **25** (5), 897–917.

HEATHCOTE, S. & GURSUL, I. 2007 Flexible flapping airfoil propulsion at low Reynolds numbers. *AIAA J.* **45** (5), 1066–1079.

HUBEL, T. Y., HRISTOV, N. I., SWARTZ, S. M. & BREUER, K. S. 2012 Changes in kinematics and aerodynamics over a range of speeds in *Tadarida brasiliensis*, the Brazilian free-tailed bat. *J. R. Soc. Interface* **9** (71), 1120–1130.

JAWORSKI, J. W. & GORDNIER, R. E. 2012 High-order simulations of low Reynolds number membrane airfoils under prescribed motion. *J. Fluids Struct.* **31**, 49–66.

JAWORSKI, J. W. & GORDNIER, R. E. 2015 Thrust augmentation of flapping airfoils in low Reynolds number flow using a flexible membrane. *J. Fluids Struct.* **52**, 199–209.

JONES, K. & PLATZER, M. 1997 Numerical computation of flapping-wing propulsion and power extraction. In *35th Aerospace Sciences Meeting and Exhibit*, p. 826. American Institute of Aeronautics and Astronautics.

KANG, C.-K. & SHYY, W. 2014 Analytical model for instantaneous lift and shape deformation of an insect-scale flapping wing in hover. *J. R. Soc. Interface* **11** (101), 20140933.

KATZ, J. & PLOTKIN, A. 2001 *Low-Speed Aerodynamics*. Cambridge University Press.

MASON, J. C. & HANDSCOMB, D. C. 2002 *Chebyshev Polynomials*. Chapman and Hall/CRC.

MEDINA, C. & KANG, C. K. 2018 An analytical solution to the aeroelastic response of a two-dimensional elastic plate in axial potential flow. *J. Fluid Mech.* **845**, R3.

MICHELIN, S. & LLEWELLYN SMITH, S. G. 2009 Resonance and propulsion performance of a heaving flexible wing. *Phys. Fluids* **21** (7), 071902.

MINAMI, H. 1998 Added mass of a membrane vibrating at finite amplitude. *J. Fluids Struct.* **12** (7), 919–932.

MOORE, M. N. J. 2014 Analytical results on the role of flexibility in flapping propulsion. *J. Fluid Mech.* **757**, 599–612.

MOORE, M. N. J. 2015 Torsional spring is the optimal flexibility arrangement for thrust production of a flapping wing. *Phys. Fluids* **27** (9), 091701.

MOORE, M. N. J. 2017 A fast Chebyshev method for simulating flexible-wing propulsion. *J. Comput. Phys.* **345**, 792–817.

MOORED, K. W., DEWEY, P. A., BOSCHITSCH, B. M., SMITS, A. J. & HAJ-HARIRI, H. 2014 Linear instability mechanisms leading to optimally efficient locomotion with flexible propulsors. *Phys. Fluids* **26** (4), 041905.

MORISON, J., JOHNSON, J. & SCHAAF, S. 1950 The force exerted by surface waves on piles. *J. Petrol. Tech.* **2** (05), 149–154.

NEWMAN, B. G. 1987 Aerodynamic theory for membranes and sails. *Prog. Aerosp. Sci.* **24** (1), 1–27.

NIELSEN, J. N. 1963 Theory of flexible aerodynamic surfaces. *Trans. ASME J. Appl. Mech.* **30** (3), 435–442.

OLIVIER, M. & DUMAS, G. 2016 A parametric investigation of the propulsion of 2D chordwise-flexible flapping wings at low Reynolds number using numerical simulations. *J. Fluids Struct.* **63**, 210–237.

PAÏDOUSSIS, M., PRICE, S. & DE LANGRE, E. 2010 *Fluid–Structure Interactions: Cross-Flow-Induced Instabilities*. Cambridge University Press.

PARAZ, F., SCHOUVEILER, L. & ELOY, C. 2016 Thrust generation by a heaving flexible foil: resonance, nonlinearities, and optimality. *Phys. Fluids* **28** (1), 011903.

PEDERZANI, J. N. & HAJ-HARIRI, H. 2006 Numerical analysis of heaving flexible airfoils in a viscous flow. *AIAA J.* **44** (11), 2773–2779.

QUINN, D. B., LAUDER, G. V. & SMITS, A. J. 2015 Maximizing the efficiency of a flexible propulsor using experimental optimization. *J. Fluid Mech.* **767**, 430–448.

https://doi.org/10.1017/jfm.2018.966 Published online by Cambridge University Press

RICHARDS, A. J. & OSHKAI, P. 2015 Effect of the stiffness, inertia and oscillation kinematics on the thrust generation and efficiency of an oscillating-foil propulsion system. *J. Fluids Struct.* **57**, 357–374.

ROJRATSIRIKUL, P., WANG, Z. J. & GURSUL, I. 2009 Unsteady fluid–structure interactions of membrane airfoils at low Reynolds numbers. *Exp. Fluids* **46** (5), 859–872.

SAAD, Y. & SCHULTZ, M. H. 1986 GMRES: a generalized minimal residual algorithm for solving nonsymmetric linear systems. *SIAM J. Sci. Stat. Comput.* **7** (3), 856–869.

SKULBORSTAD, A. J., SWARTZ, S. M. & GOULBOURNE, N. C. 2015 Biaxial mechanical characterization of bat wing skin. *Bioinspir. Biomim.* **10** (3), 036004.

SMITH, R. & SHYY, W. 1995*a* Computation of unsteady laminar flow over a flexible two-dimensional membrane wing. *Phys. Fluids* **7** (9), 2175–2184.

SMITH, R. & SHYY, W. 1995*b* Computational model of flexible membrane wings in steady laminar flow. *AIAA J.* **33** (10), 1769–1777.

SMITH, R. & SHYY, W. 1996 Computation of aerodynamic coefficients for a flexible membrane airfoil in turbulent flow: a comparison with classical theory. *Phys. Fluids* **8** (12), 3346–3353.

SONG, A., TIAN, X., ISRAELI, E., GALVAO, R., BISHOP, K., SWARTZ, S. & BREUER, K. 2008 Aeromechanics of membrane wings with implications for animal flight. *AIAA J.* **46** (8), 2096–2106.

SPAGNOLIE, S. E., MORET, L., SHELLEY, M. J. & ZHANG, J. 2010 Surprising behaviors in flapping locomotion with passive pitching. *Phys. Fluids* **22** (4), 041903.

THEODORSEN, T. 1935 General theory of aerodynamic instability and the mechanism of flutter. *NACA Tech. Rep.* 496.

THOMSON, W. 1996 *Theory of Vibration with Applications*. CRC Press.

THWAITES, B. 1961 The aerodynamic theory of sails. I. Two-dimensional sails. *Proc. R. Soc. Lond.* A **261** (1306), 402–422.

TRIANTAFYLLOU, M. S., TRIANTAFYLLOU, G. S. & GOPALKRISHNAN, R. 1991 Wake mechanics for thrust generation in oscillating foils. *Phys. Fluids* A **3** (12), 2835–2837.

WALDMAN, R. M. & BREUER, K. S. 2017 Camber and aerodynamic performance of compliant membrane wings. *J. Fluids Struct.* **68**, 390–402.

WU, T. Y.-T. 1961 Swimming of a waving plate. *J. Fluid Mech.* **10** (3), 321–344.

ZHANG, J., LIU, N. S. & LU, X. Y. 2010 Locomotion of a passively flapping flat plate. *J. Fluid Mech.* **659**, 43–68.

https://doi.org/10.1017/jfm.2018.966 Published online by Cambridge University Press